Bibliography

1 PEDEN, M.; SCURFIELD, R.; SLEET, D. ; ET AL.. **World report on road traffic injury prevention**. World Health Organization, Geneva, 2004.

2 ORGANIZATION, W. H.. **Global status report on road safety 2015**. World Health Organization, 2015.

3 COMMISSION, E.. **Traffic safety basic facts on main figures**. Technical report, Directorate General for Transport, June 2016.

4 EVANS, L.. **The dominant role of driver behavior in traffic safety.** American Journal of Public Health, 86(6):784–786, 1996.

5 PETRIDOU, E.; MOUSTAKI, M.. **Human factors in the causation of road traffic crashes**. European journal of epidemiology, 16(9):819–826, 2000.

6 ERKE, A.. **Effects of electronic stability control (esc) on accidents: A review of empirical evidence**. Accident Analysis & Prevention, 40(1):167–173, 2008.

7 MOBILITEIT, B.-R.. **Mobiliteit in cijfers auto's 2013/2014**. Technical report, BOVAG-RAI, 2014.

8 GORDON, T.; HOWELL, M. ; BRANDAO, F.. **Integrated control methodologies for road vehicles**. Vehicle System Dynamics, 40(1-3):157–190, 2003.

9 MAGNUS, K.. **Dynamics of Multibody Systems: Symposium Munich/Germany August 29–September 3, 1977**. Springer Science & Business Media, 2012.

10 SONG, P.. **Modeling, analysis and simulation of multibody systems with contact and friction**. PhD thesis, University of Pennsylvania, 2002.

11 KORTÜM, W.. **Review of multibody computer, codes for vehicle system dynamics**. Vehicle system dynamics, 22(S1):3–31, 1993.

12 VON SCHWERIN, R.. **Multibody system simulation: numerical methods, algorithms, and software**, volumen 7. Springer Science & Business Media, 2012.

13 PASTORINO, R.; DOPICO, D.; SANJURJO, E. ; NAYA, M. Á.. **Validation of a multibody model for an x-by-wire vehicle prototype through field testing**. In: PROCEEDINGS OF THE MULTIBODY DYNAMICS 2011, ECCOMAS THEMATIC CONFERENCE, p. 144–145, 2011.

14 CARVALHO, M.; AMBRÓSIO, J. ; EBERHARD, P.. **Identification of validated multibody vehicle models for crash analysis using a hybrid optimization procedure**. Structural and Multidisciplinary Optimization, 44(1):85–97, 2011.

15 MAIER, O.; GYÖRFI, B.; WREDE, J. ; KASPER, R.. **Design and validation of a multi-body model of a front suspension bicycle and a passive rider for braking dynamics investigations**. Multibody System Dynamics, p. 1–27, 2017.

16 RILL, G.; FAISST, H.; HAUTMANN, J. ; ERTLMEIER, R.. **Vehicle rollover in off-road conditions**. The Dynamics of Vehicles on Road and on Tracks, IAVSD 09, (Stockholm, Sweden), 2009.

17 BLUNDELL, M.; HARTY, D.. **The multibody systems approach to vehicle dynamics**. Elsevier, 2004.

18 KEEN, S. D.; COLE, D. J.. **Steering control using model predictive control and multiple internal models**. In: PROCEEDINGS OF THE 8TH INTERNATIONAL SYMPOSIUM ON AUTOMOTIVE CONTROL (AVEC 2006), p. 599–604, 2006.

19 REIF, K.. **Fundamentals of automotive and engine technology**. Springer: Bosch professional automotive information, 2014.

20 GMBH, R. B.. **From innovation to standard equipment 30 years of safe braking with bosch abs**, July 2008.

21 KESHMIRI, R.; SHAHRI, A. M.. **Intelligent abs fuzzy controller for diverse road surfaces**. World Academy of Science, Engineering and Technology, 2(2):62–67, 2007.

22 GUO, J.; JIAN, X. ; LIN, G.. **Performance evaluation of an anti-lock braking system for electric vehicles with a fuzzy sliding mode controller**. Energies, 7(10):6459–6476, 2014.

23 CHIN, Y.-K.; LIN, W. C.; SIDLOSKY, D. M.; RULE, D. S. ; SPARSCHU, M. S.. **Sliding-mode abs wheel-slip control**. In: AMERICAN CONTROL CONFERENCE, 1992, p. 1–8. IEEE, 1992.

24 BUCKHOLTZ, K. R.. **Reference input wheel slip tracking using sliding mode control**. Technical report, SAE Technical Paper, 2002.

25 TANELLI, M.; ASTOLFI, A. ; SAVARESI, S. M.. **Robust nonlinear output feedback control for brake by wire control systems**. Automatica, 44(4):1078–1087, 2008.

26 BASLAMISLI, S. C.; KÖSE, I. E. ; ANLAŞ, G.. **Robust control of anti-lock brake system**. Vehicle System Dynamics, 45(3):217–232, 2007.

27 KOBAYASHI, K.; CHEOK, K. C. ; WATANABE, K.. **Estimation of absolute vehicle speed using fuzzy logic rule-based kalman filter**. In: AMERICAN CONTROL CONFERENCE, PROCEEDINGS OF THE 1995, volumen 5, p. 3086–3090. IEEE, 1995.

28 VILLAGRA, J.; D'ANDREA NOVEL, B.; FLIESS, M. ; MOUNIER, H.. **Estimation of longitudinal and lateral vehicle velocities: an algebraic approach**. In: AMERICAN CONTROL CONFERENCE, 2008, p. 3941–3946. IEEE, 2008.

29 MOAVENI, B.; KHOSRAVI ROQAYE ABAD, M. ; NASIRI, S.. **Vehicle longitudinal velocity estimation during the braking process using unknown input kalman filter**. Vehicle System Dynamics, 53(10):1373–1392, 2015.

30 PASILLAS-LÉPINE, W.. **Hybrid modeling and limit cycle analysis for a class of five-phase anti-lock brake algorithms**. Vehicle System Dynamics, 44(2):173–188, 2006.

31 GERARD, M.. **Global chassis control and braking control using tyre forces measurement**. PhD thesis, Technische Universiteit Delft, 2011.

32 LEE, T.-T.; HSU, C.-F. ; LEE, S.. **Robust hybrid control for antilock braking systems**. In: SYSTEMS, MAN AND CYBERNETICS, 2003. IEEE INTERNATIONAL CONFERENCE ON, volumen 1, p. 84–89. IEEE, 2003.

33 RILL, G.. **Road vehicle dynamics: fundamentals and modeling**. CRC Press, 2011.

34 MANNING, W.; CROLLA, D.. **A review of yaw rate and sideslip controllers for passenger vehicles**. Transactions of the Institute of Measurement and Control, 29(2):117–135, 2007.

35 MATSUMOTO, S.; YAMAGUCHI, H.; INOUE, H. ; YASUNO, Y.. **Improvement of vehicle dynamics through braking force distribution control**. Technical report, SAE Technical Paper, 1992.

36 KRAEMER, W.; HACKL, M.. **Potential functions and benefits of electronic steering assistance**. In: XXVI FISISTA CONGRESS,(PRAHA), 1996.

37 SHIBAHATA, Y.; SHIMADA, K. ; TOMARI, T.. **Improvement of vehicle maneuverability by direct yaw moment control**. Vehicle system dynamics, 22(5-6):465–481, 1993.

38 SHIMADA, K.; SHIBAHATA, Y.. **Comparison of three active chassis control methods for stabilizing yaw moments**. Technical report, SAE Technical Paper, 1994.

39 FURUKAWA, Y.; YUHARA, N.; SANO, S.; TAKEDA, H. ; MATSUSHITA, Y.. **A review of four-wheel steering studies from the viewpoint of vehicle dynamics and control**. Vehicle system dynamics, 18(1-3):151–186, 1989.

40 HIRANO, Y.; FUKATANI, K.. **Development of robust active rear steering control for automobile**. JSME International Journal Series C Mechanical Systems, Machine Elements and Manufacturing, 40(2):231–238, 1997.

41 CHATZIKOMIS, C.; SPENTZAS, K.. **Comparison of a vehicle equipped with electronic stability control (esc) to a vehicle with four wheel steering (4ws)**. Forschung im Ingenieurwesen, 78(1-2):13–25, 2014.

42 SORNIOTTI, A.; MORGANDO, A. ; VELARDOCCHIA, M.. **Active roll control: system design and hardware-in-the-loop test bench**. Vehicle System Dynamics, 44(sup1):489–505, 2006.

43 CRONJE, P. H.; ELS, P. S.. **Improving off-road vehicle handling using an active anti-roll bar**. Journal of Terramechanics, 47(3):179–189, 2010.

44 ZULKARNAIN, N.; IMADUDDIN, F.; ZAMZURI, H. ; MAZLAN, S. A.. **Application of an active anti-roll bar system for enhancing vehicle**

ride and handling. In: HUMANITIES, SCIENCE AND ENGINEERING (CHUSER), 2012 IEEE COLLOQUIUM ON, p. 260–265. IEEE, 2012.

45 CASTRO, A. A.; CHAVES, R. B.; RILL, G. ; WEBER, H. I.. **Use of integrated control to enhance the safety of vehicles in run-off-road scenarios**. In: XVII INTERNATIONAL SYMPOSIUM ON DYNAMIC PROBLEMS OF MECHANICS, 2017.

46 CASTRO, A.; RILL, G. ; WEBER, H. I.. **Development of a robust integrated control system to improve the stability of road vehicles**. In: INTERNATIONAL SYMPOSIU ON MULTIBODY SYSTEMS AND MECHATRONICS, p. 506–516. Springer, 2017.

47 VILELA, D.; BARBOSA, R. S.. **Analytical models correlation for vehicle dynamic handling properties**. Journal of the Brazilian Society of Mechanical Sciences and Engineering, 33(4):437–444, 2011.

48 EVERS, W.. **Improving driver comfort in commercial vehicles: Modeling and control of a low-power active cabin suspension system**. Eindhoven, The Netherlands: Eindhoven University of Technology, 2010.

49 PENNESTRI, E.; VALENTINI, P. P. ; VITA, L.. **Comfort analysis of car occupants: comparison between multibody and finite element models**. International Journal of Vehicle Systems Modelling and Testing, 1(1-3):68–78, 2005.

50 NIKRAVESH, P. E.. **Computer-aided analysis of mechanical systems**. Prentice-Hall, Inc., 1988.

51 GIPSER, M.. **Ftire: a physically based application-oriented tyre model for use with detailed mbs and finite-element suspension models**. Vehicle system dynamics, 43(sup1):76–91, 2005.

52 RILL, G.. **Sophisticated but quite simple contact calculation for handling tire models**. In: EUROMECH COLLOQUIUM 578, ROLLING CONTACT MECHANICS FOR MULTIBODY SYSTEM DYNAMICS, MADEIRA, PORTUGAL, 2017.

53 RILL, G.. **An engineer's guess on tyre model parameter made possible with tmeasy**. In: INTERNATIONAL TYRE COLLOQUIUM, 4TH, 2015, GUILDFORD, UNITED KINGDOM, 2015.

54 PACEJKA, H.. **Tire and vehicle dynamics**. Elsevier, 2005.

55 BENEKOHAL, R.; TREITERER, J.. **Carsim: Car-following model for simulation of traffic in normal and stop-and-go conditions**. Transportation research record, (1194), 1988.

56 **Adams car**. `http://www.mscsoftware.com.br/product/adams-car`. Accessed: 2017-09-30.

57 **Vi-carrealtime**. `https://www.vi-grade.com/en/products/vi-carrealtime/`. Accessed: 2017-09-30.

58 JONES, E.; OLIPHANT, T.; PETERSON, P. ; OTHERS. **SciPy: Open source scientific tools for Python**, 2001. [Online; accessed 2017-08-01].

59 WALT, S. V. D.; COLBERT, S. C. ; VAROQUAUX, G.. **The numpy array: a structure for efficient numerical computation**. Computing in Science & Engineering, 13(2):22–30, 2011.

60 HUNTER, J. D.. **Matplotlib: A 2d graphics environment**. Computing In Science & Engineering, 9(3):90–95, 2007.

61 HAIRER, E.; WANNER, G. ; OTHERS. **Solving ordinary differential equations II: Stiff and differential-algebraic problems**. Springer, 1996.

62 HAIRER, E.; WANNER, G.. **Solving ordinary differential equations. ii, volume 14 of springer series in computational mathematics**, 1996.

63 RILL, G.. **Simulation von Kraftfahrzeugen**. Vieweg Braunschweig, 1994.

64 POPP, K.; SCHIEHLEN, W.. **Ground vehicle dynamics**. Springer Science & Business Media, 2010.

65 BROWN, P. N.; BYRNE, G. D. ; HINDMARSH, A. C.. **Vode: A variable-coefficient ode solver**. SIAM journal on scientific and statistical computing, 10(5):1038–1051, 1989.

66 VOLKSWAGEN; AUDI. **Electronic stability programme: Design and function**. Technical report, Volkswagen & Audi, 2004.

67 RILL, G.; SCHAEFFER, T.. **Grundlagen und Methodik der Mehrkörpersimulation**. Springer, 2010.

68 ROBERSON, R. E.; SCHWERTASSEK, R.. **Dynamics of multibody systems**. Springer Science & Business Media, 2012.

69 GENTA, G.; GENTA, A.. **Road Vehicle Dynamics: Fundamentals of Modeling and Simulation**, volumen 88. World Scientific, 2016.

70 REIF, K.. **Automotive Mechatronics: Automotive Networking, Driving Stability Systems, Electronics**. Springer, 2014.

71 BOBIER, C. G.. **A phase portrait approach to vehicle stabilization and envelope control**. PhD thesis, Stanford University, 2012.

A
Double wishbone suspension kinematic constraints

A.1
Constraint equations: wheel up/down motion

In order to satisfy the suspension topology, constraint equations are need to be considered in the kinematic model. Similarly to the wheel's position, the position of the ball joint F can be expressed in the vehicle-fixed axis system V, see Figure 47, as follows

$$r_{VF,V} = r_{VB,V} + A_{\phi} r_{BC,\phi} + A_{VW} r_{CF,W} \tag{A-1}$$

where $r_{VB,V}$ (measured in V), $r_{BC,\phi}$ (measured in an axis system fixed to the lower control arm) and $r_{CF,W}$ (measured in the wheel-fixed axis system W) are defined by the suspension topology. Furthermore, because F is also attached to the upper control arm, its position can be also represented by,

$$r_{VF,V} = r_{VD,V} + A_{\rho} r_{DF,\rho} \tag{A-2}$$

where $r_{VD,V}$ (measured in V) and $r_{DF,\rho}$ (measured in an axis system fixed to the upper control arm) are given by data and, A_ρ represent the rotation matrix of the upper control arm. Similarly to Equation 2-21, A_ρ can be calculated using the rotation axis e_ρ (defined by D and E) via

$$A_{\rho} = e_{\rho} e_{\rho}^{T} + \left(I_{3\times3} - e_{\rho} e_{\rho}^{T} \right) \cos\rho + \tilde{e}_{\rho} \sin\rho. \tag{A-3}$$

where ρ is the angle of rotation around e_ρ as illustrated in Figure 47.

Considering and rearranging Equation A-1, A-2 and A-3, it is possible to find an expression of the form

$$a\cos\rho + b\sin\rho = c \tag{A-4}$$

with

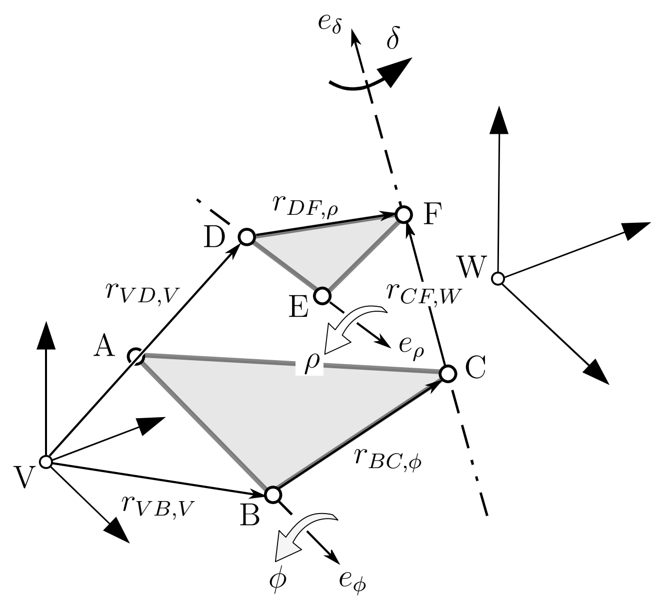

Figure 47: Lower and upper control arms of a double wishbone suspension system.

$$
\begin{aligned}
a &= r_{CD,V}^T \left(I_{3\times3} - e_\rho e_\rho^T\right) r_{DF,\rho} \\
b &= r_{CD,V}^T \, e_\rho \times r_{DF,\rho} \\
c &= \tfrac{1}{2}\left[\overline{CF}^2 - \left(\overline{CD}^2 + \overline{DF}^2\right)\right] - r_{CD,V}^T \, e_\rho e_\rho^T \, r_{DF,\rho} \\
r_{CD,V} &= r_{VD,V} - \left(r_{VB,V} + A_\phi r_{BC,\phi}\right)
\end{aligned}
\tag{A-5}
$$

where $\overline{CF}$ and $\overline{DF}$ are the lengths of the vectors r_{CF} and r_{DF} respectively, and $\overline{CD} = r_{CD,V}^T r_{CD,V}$. The solution of the Equation A-4 can be easily obtained via

$$
\rho = \arcsin\left(\frac{c}{\sqrt{a^2+b^2}}\right) - \arctan\left(\frac{a}{b}\right) \tag{A-6}
$$

where $\rho = \rho(\phi)$ because $r_{CD,V}$ is function of ϕ as presented in Equation A-5. With $\rho = \rho(\phi)$, the rotation matrix of the upper control arm A_ρ can be calculated using Equation A-3, i.e. $A_\rho(\phi)$. Then, the rotation of the upper control arm is completely described by the rotation of the lower control arm ϕ.

The next step is to obtain an expression of the elementary rotation A_α and A_β in function of the ϕ. This is required in order to describe the wheel body orientation under pure up/down wheel motion, i.e. variation of ϕ. The vector $r_{CF,V}$ can be expressed by,

$$r_{CF,V} = r_{CD,V}(\phi) + A_\rho(\phi) r_{DF,\rho} \tag{A-7}$$

where $r_{CD,V}$ is obtained from Equation A-5 and $A_\rho(\phi)$ from Equation A-3. In addition, $r_{CF,V}$ can be also calculated by using the elementary rotations as follows

$$A_\alpha A_\beta A_\delta r_{CF,W} = r_{CF,V}. \tag{A-8}$$

However, because $r_{CF,W}$ coincides with the rotation axis e_δ, it will be not affected by this rotation, i.e. $A_\delta r_{CF,W} = r_{CF,W}$. Then, using this last equality into Equation A-8, it is obtained

$$A_\alpha A_\beta r_{CF,W} = r_{CF,V} \tag{A-9}$$

where $r_{CF,V}$ is calculated using Equation A-7. Then, by multiplying the last equation by A_α^T and considering Equation 2-23, we obtain

$$\begin{bmatrix} \cos\beta & 0 & \sin\beta \\ 0 & 1 & 0 \\ -\sin\beta & 0 & \cos\beta \end{bmatrix} r_{CF,W} = \begin{bmatrix} 1 & 0 & 0 \\ 0 & \cos\alpha & -\sin\alpha \\ 0 & \sin\alpha & \cos\alpha \end{bmatrix}^T r_{CF,V} \tag{A-10}$$

where $r_{CF,W}$ is measured in the wheel-fixed axis system W and is given by data, and $r_{CF,W}$ is know from Equation A-7. Equation A-10 is a system of equations with two unknown variables, i.e. α and β. Then, considering the 1st and 3rd row of this equation system, it is possible to find mathematical expressions, similarly to Equation A-4, for α and β. Consequently, they can be solved by using Equation A-6. Finally, the upper control arm rotation ρ (Equation A-6), and the elementary rotations α and β (Equation A-10) are described by the wheel up/down motion, i.e. the rotation of the lower control arm ϕ.

A.2
Constraint equations: rack displacement

For the suspension model presented here, a pure lateral rack motion was assumed. In addition, the rack displacement commands the wheel rotation around the kingpin axis e_ρ through the drag link. Then, the actual position of the ball joint R can be expressed in the vehicle-fixed axis system V as follows

$$r_{VR,V} = r^K_{VR,V} + \begin{bmatrix} 0 \\ u_F \\ 0 \end{bmatrix} \tag{A-11}$$

where $r^K_{VR,V}$ represents the design position of the ball joint R related to V and is defined by the topology of the suspension, and u_F is the front rack displacement.

The other attached point of the drag link, i.e. the ball joint Q, can be calculated via

$$r_{VQ,V} = r_{VA,V} + A_\phi r_{AC,\phi} + A_{VW} r_{CQ,W} \tag{A-12}$$

where $r_{VA,V}$ (measured in V), $r_{AC,\phi}$ (measured in an axis system fixed to the lower control arm) and $r_{CQ,W}$ (measured in the wheel-fixed axis system W) are defined by the suspension topology. Considering the current position of the attached points of the drag link, i.e. R and Q, it is possible to defined the second constraint equation via

$$(r_{VQ,V} - r_{VR,V})^T (r_{VQ,V} - r_{VR,V}) = \overline{RQ}^2 \tag{A-13}$$

where $r_{VR,V}$ and $r_{VQ,V}$ are obtained using Equation A-11 and A-12 respectively, and $\overline{RQ}$ is the length of the drag link.

From the suspension topology, see Figure 15, it is possible to define the position of the ball joint C as follows

$$r_{VC,V} = r_{VR,V} + r_{RC,V} = r_{VA,V} + A_\phi r_{AC} \tag{A-14}$$

Then, inserting the previous expression into Equation A-12, we obtain

$$r_{VQ,V} - r_{VR,V} = r_{RC,V} + A_{VW} r_{CQ,W} \tag{A-15}$$

Finally, inserting the last expression into the Equation A-13, one gets

$$(r_{RC,V} + A_{VW} r_{CQ,W})^T (r_{RC,V} + A_{VW} r_{CQ,W}) = \overline{RQ}^2 \tag{A-16}$$

rearranging and simplifying last expression results in

$$r^T_{RC,V} r_{RC,V} + 2 r^T_{RC,V} A_{VW} r_{CQ,W} + r^T_{CQ,W} r_{CQ,W} = \overline{RQ}^2 \tag{A-17}$$

Using the the previous equation and considering the following: $A_{VW} = A_\alpha A_\beta A_\delta$ and A_δ is defined by Equation 2-23, $\overline{RC} = r_{RC,V}^T r_{RC,V}$ and $\overline{CQ} = r_{CQ,W}^T r_{CQ,W}$, it is obtained an expression similarly of Equation A-4 and therefore, it can be solved using Equation A-6.

B
Steering tendencies

In order to analyze the steering tendency of road vehicles, a driving maneuver called steady state cornering is performed. For this maneuver, a human driver or an appropriate driver model, see Section 3, need to maintain the vehicle on a curve of radius R and at the same time increase slowly the driving speed v. As the lateral acceleration can be computed via $a_y = v^2/R$, it also increases when v increases until reaching the tire-road adhesion limit. Depending of which tires saturates first, i.e. front or rear tires, the vehicle reaches the oversteer or understeer limit.

B.1
Scaled car

In Figure 48, the steering wheel angle and the sideslip angle of the scaled car (employed to validate the lateral dynamics of the multibody vehicle model) against the lateral acceleration at the vehicle COG are shown. Table 11 summarize the characteristic parameters of the SHM for the scaled car.

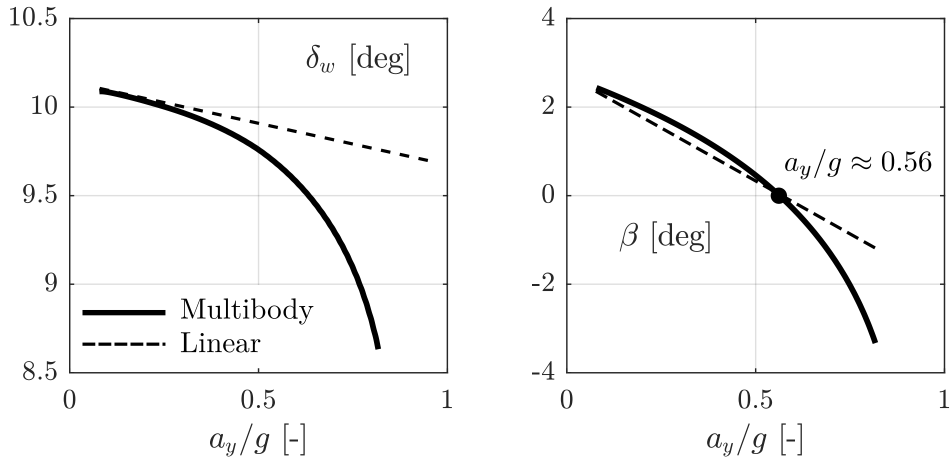

Figure 48: Steering tendency of the scaled car.

It can be noticed from the left plot that the scaled car has a highly oversteer tendency. With this characteristic the vehicle becomes unstable with a tendency to spin out. However, some skilled drivers prefer this type of vehicle in order to perform drastic driving maneuvers, e.g. drifting.

Table 11: Scaled car: characteristic parameters for the corresponding SHM

Parameter	**Symbol**	**Value**	**Unit**
Vehicle mass	m	10.54	kg
Vehicle z-axis inertia	Θ	1.05	kg.m^2
Distance COG to front axle	l_f	0.31	m
Distance COG to rear axle	l_r	0.22	m
Cornering stiffness at front axle	K_f	625	N/m
Cornering stiffness at rear axle	K_r	775	N/m

B.2
Fullsize car

Figure 49, shows the steering tendency of a fullsize car. The solid line represents the steering wheel angle computing using the fully nonlinear and three-dimensional multibody vehicle model with the characteristic parameters summarized in Table 8, and the dashed line was computed using a SHM with a linear tire model considering the front and rear cornering stiffness, see Table 12. The front and rear cornering stiffness, K_f and K_r in Table 12 respectively, describe the stiffness of each axle, that depends for example, on the suspension configuration and tire force characteristics. As can be noticed from the left plot of the Figure 49, the fullsize car has an understeer tendency, i.e. $K_r l_r > K_f l_f$.

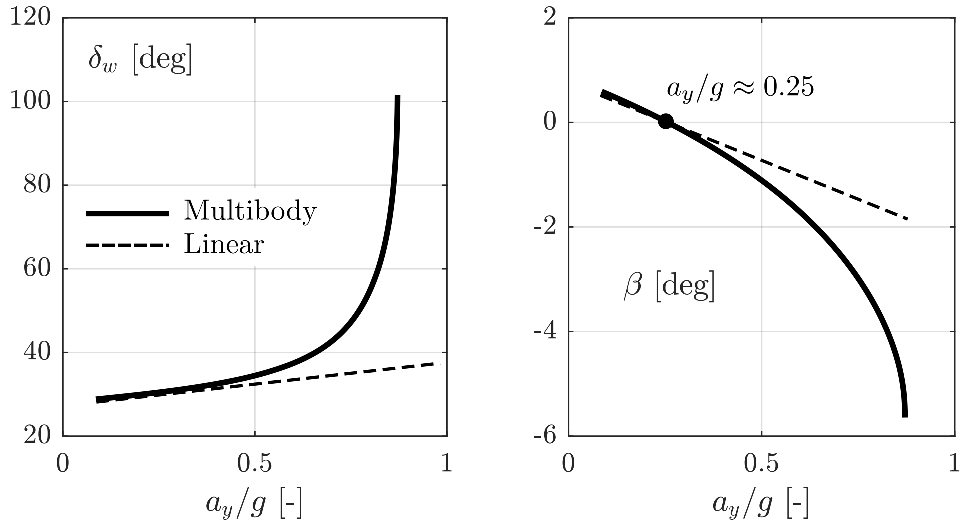

Figure 49: Steering tendency of a fullsize car.

Table 12: Fullsize car: characteristic parameters for the corresponding SHM

Parameter	Symbol	Value	Unit
Vehicle mass	m	2127.8	kg
Vehicle z-axis inertia	Θ	3358.3	kg.m^2
Distance COG to front axle	l_f	1.5	m
Distance COG to rear axle	l_r	1.4	m
Cornering stiffness at front axle	K_f	150	kN/m
Cornering stiffness at rear axle	K_r	200	kN/m

B.3 Midsize car

Figure 50 shows the steering tendency of a midsize car. Characteristic parameters employing for the SHM of the midsize car are summarized in Table 13. As can be noticed in Figures 49 and 50, these type of vehicles have an understeer tendency. This is normal for passengers car because, although the vehicle follows a path of radius larger than the driver intends, it is dynamically stable [33].

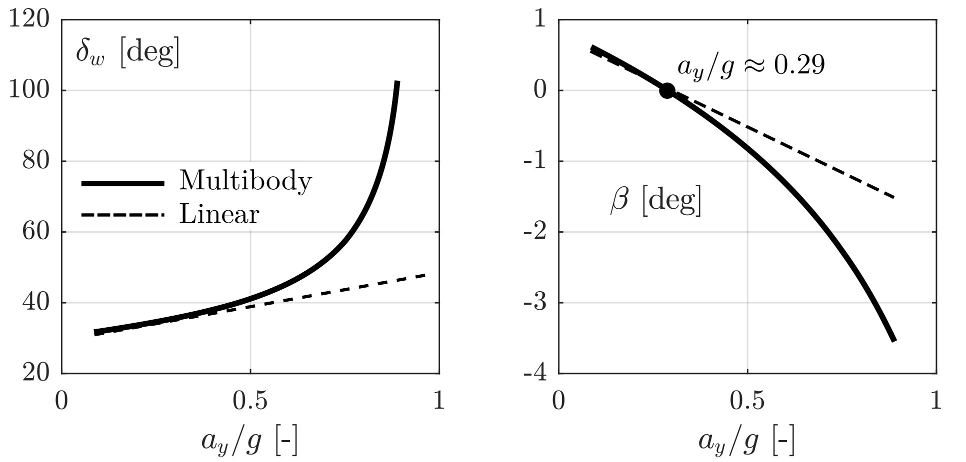

Figure 50: Steering tendency of a midsize car.

Table 13: Midsize car: characteristic parameters for the corresponding SHM

Parameter	Symbol	Value	Unit
Vehicle mass	m	1450	kg
Vehicle z-axis inertia	Θ	2020.3	kg.m^2
Distance COG to front axle	l_f	1.13	m
Distance COG to rear axle	l_r	1.47	m
Cornering stiffness at front axle	K_f	121.5	kN/m
Cornering stiffness at rear axle	K_r	120	N/m